Imaging Endothelin ET_B Receptors Using [^{18}F]-BQ3020: *In Vitro* Characterization and Positron Emission Tomography (MicroPET)

PETER JOHNSTRÖM,*,[1] JAMES H. F. RUDD,† HUGH K. RICHARDS,‡ TIM D. FRYER,§ JOHN C. CLARK,§ PETER L. WEISSBERG,† JOHN D. PICKARD,‡,§ AND ANTHONY P. DAVENPORT*

**Clinical Pharmacology Unit, †Division of Cardiovascular Medicine, ‡Academic Neurosurgery, and §Wolfson Brain Imaging Centre, University of Cambridge, Addenbrooke's Hospital, Cambridge CB2 2QQ, United Kingdom*

The endothelin (ET) receptor system has been shown to play a role in a number of vascular diseases. We have synthesized ^{18}F- and ^{11}C-labeled radioligands to enable *in vivo* imaging of the fundamental processes involved in ET receptor pharmacology in normal and diseased tissue using positron emission tomography (PET). One aim is to elucidate the proposed role of the ET_B subtype as clearing receptor, removing ET-1 from the circulation, and whether this is an important mechanism to limit the detrimental effects caused by upregulated ET-1 in disease. To image ET_B receptors we have labeled the selective agonist BQ3020 with ^{18}F. *In vitro* characterization verified that [^{18}F]-BQ3020 bound with a single subnanomolar affinity ($K_D = 0.34 \pm 0.10$ n*M*, $B_{max} = 9.23 \pm 3.70$ fmol/mg protein) to human left ventricle. Binding of [^{18}F]-BQ3020 to human kidney was inhibited by ET-1 and unlabeled BQ3020 but not by the ET_A selective antagonist FR139317, confirming that selectivity for the ET_B receptor was retained. *In vitro* autoradiography revealed, as expected, high levels of ET_B receptor densities in lung and kidney medulla, whereas kidney cortex and heart showed lower levels of ET_B receptor densities. Furthermore, a high level of [^{18}F]-BQ3020 binding was found to colocalize to macrophages in atherosclerotic coronary arteries. MicroPET studies demonstrated high uptake of [^{18}F]-BQ3020 in ET_B receptor–rich tissue, including lung, liver and kidney. The *in vivo* biodistribution of [^{18}F]-BQ3020 was comparable to that previously obtained for [^{18}F]-ET-1, supporting our hypothesis that the ET_B receptor plays a significant role in the uptake of ET-1. In conclusion, [^{18}F]-BQ3020 has retained high affinity and selectivity, allowing imaging of ET_B receptor distributions *in vitro* and *in vivo* in human and animal tissue. Furthermore, *in vitro* data suggest that [^{18}F]-BQ3020 potentially can be used to image atherosclerotic lesions *in vivo* using PET. Exp Biol Med 231:736–740, 2006

Key words: endothelin; ET_B receptors; positron emission tomography; microPET; ^{18}F; *in vivo* imaging

Introduction

Positron emission tomography (PET) is the most sensitive technique for imaging and quantifying receptor-bound radioligands *in vivo*. With the recent introduction of dedicated PET scanners for small animals, such as the microPET, it is now possible to perform functional imaging in rodents at high resolution (<2 mm), enabling delineation of receptor distributions within discrete organs and their larger substructures.

Vascular receptors for peptides such as endothelin (ET) are a diverse group of potential drug targets that have not been studied extensively using PET. We have recently demonstrated that binding to ET receptors in rat can be imaged dynamically using the microPET (1). Our aim is to use microPET to image the ET receptor system *in vivo* to elucidate the fundamental processes involved in ET receptor pharmacology in normal and diseased tissue, and particularly the role of the ET_B receptor subtype in tissues including lung, kidney, and liver, where high densities of this subtype are expressed. We hypothesize that tissue-specific removal of circulating ET-1 is mediated by ET_B receptors and that this will be an important mechanism to limit the detrimental effects caused by upregulated ET-1 in disease.

To enable PET imaging of both receptor subtypes (ET_A and ET_B), we have labeled the endogenous ligand ET-1 and the mixed antagonist SB209670 with ^{18}F (2, 3). In addition, the ET_A selective antagonist PD156707 and the precursor peptide big ET-1 have been labeled with ^{11}C and ^{18}F,

This work was supported by grants from the British Heart Foundation, the Medical Research Council Technology Foresight (U.K. Government), and, for the microPET, a JREI grant from HEFCE and Merck Sharp & Dohme, Ltd.

[1] To whom correspondence should be addressed at Clinical Pharmacology Unit, University of Cambridge, Addenbrooke's Centre for Clinical Investigation, Level 6, Box 110, Addenbrooke's Hospital, Cambridge CB2 2QQ, United Kingdom. E-mail: pjj20@medschl.cam.ac.uk

Received September 29, 2005.
Accepted November 10, 2005.

1535-3702/06/2316-0736$15.00

Table 1. Dissociation Constant (K_D), Maximal Density of Receptors (B_{max}), and Hill Coefficient (nH) for [^{18}F]-BQ3020 in Human Left Ventricle[a]

	K_D (n*M*)	B_{max} (fmol/mg proteins)	nH	Reference
[^{18}F]-BQ3020	0.34 ± 0.10	9.23 ± 3.70	0.84 ± 0.12	—
[^{125}I]-BQ3020	0.107 ± 0.004	18.9 ± 4.8	0.43 ± 0.06	10
[^{18}F]-ET-1	0.43 ± 0.05	27.8 ± 2.1	0.95 ± 0.04	1

[a] $n = 4$. Values are mean ± SEM. For comparison, values for [^{125}I]-BQ3020 and [^{18}F]-ET-1 are included.

respectively (4, 5), to allow imaging of ET_A receptors and enzyme conversion of big ET-1 to ET-1 *in vivo*. To image the ET_B subtype, the selective agonist BQ3020 was labeled with ^{18}F (4). The purpose of the present study was to validate that the label was tolerated using *in vitro* receptor binding characterization, as well as to perform initial microPET imaging in the rabbit to verify that the *in vivo* biodistribution of [^{18}F]-BQ3020 reflected binding to tissue expressing high densities of ET_B receptors.

Materials and Methods

Peptides and Radiolabeled Compounds. ET-1 and BQ3020 ([$Ala^{11,15}$]Ac-ET-$1_{(6–21)}$) were obtained from Peptide Institute Inc. (Osaka, Japan) and Neosystem (Strasbourg, France), respectively. FR139317 was synthesized by Dr. A. M. Doherty (Parke-Davis Pharmaceuticals Research Division, Ann Arbor, MI). [^{18}F]-BQ3020 was labeled in the ε-amino group of Lys^9 by conjugation with the Bolton-Hunter type reagent *N*-succinimidyl 4-[^{18}F]-fluorobenzoate (4).

***In Vitro* Characterization.** Cryostat sections (30 μm) were cut from the left ventricular wall and from atherosclerotic coronary arteries from explanted hearts of recipient patients undergoing cardiac transplantation, from normal renal tissue (containing cortex and medulla) obtained from the opposite pole to the nonobstructing tumors following nephrectomy, and from normal lung tissue from patients undergoing lobectomy for carcinoma. All tissues were obtained with local ethical approval.

[^{18}F]-BQ3020 was characterized using ligand binding assays as described previously (6). For saturation experiments, sections of human left ventricle were incubated with increasing concentrations of [^{18}F]-BQ3020 (5 p*M*–2 n*M*) for 60 mins. In inhibition experiments, sections of kidney were incubated with a fixed concentration of [^{18}F]-BQ3020 (0.5 n*M*). Inhibition of binding was tested by co-incubation with 1 μ*M* FR139317 (ET_A selective antagonist) and 1 μ*M* unlabeled BQ3020 (ET_B selective agonist), respectively. For autoradiographic visualization of ET_B receptor densities in normal tissue (heart, lung, and kidney) and diseased tissue (atherosclerotic coronary arteries), sections were incubated with a fixed concentration of [^{18}F]-BQ3020 (0.4 and 0.5 n*M*, respectively). Nonspecific binding in all assays was defined by co-incubating adjacent sections with ET-1 (1 μ*M*). Specifically-bound ligand was measured by gamma counting or by apposing the tissue to a storage phosphor imaging screen for autoradiographic analysis. Binding was quantified using ^{18}F standard curves for gamma counting or by coexposing the standards with the tissue sections.

To enable histologic examination of atherosclerotic coronary arteries, adjacent sections to those used in autoradiography were stained with hematoxylin-eosin and to visualize the presence of macrophages, a monoclonal mouse anti-human antibody (CD68) and methods described previously were used (7).

Data are expressed as mean ± SEM. Data from the saturation experiments were fitted to a one- or two-site model using nonlinear iterative curve fitting (8). A two-site model was accepted only if it resulted in a significantly better fit as judged by an *F* test ($P < 0.05$).

MicroPET Imaging. PET imaging was performed in two New Zealand White rabbits using a microPET P4 scanner (Concorde Microsystems, Knoxville, TN). All experiments were performed in accordance with the United Kingdom Animal Scientific Procedures Act, 1986, and complied with guidelines of the local animal ethics committee.

General anesthesia was used during surgery and PET imaging. Induction was achieved using intravenous alphaxalone/alphadalone (0.2 ml/kg; Schering-Plough, Welwyn Garden City, UK) diluted in saline to a volume of 5 ml, and anesthesia was maintained with a mixture of isofluorane (2.5–4%), nitrous oxide (0.8–1 liters/min), and oxygen (0.5 liters/min), delivered by secured face mask. There was no need for endotracheal intubation during any of the surgical or imaging sessions. Rectal temperature was monitored and the animal placed on a padded warming blanket. An ear vein was cannulated for administration of [^{18}F]-BQ3020 and the rabbits were then placed prone on the scanning bed. [^{18}F]-BQ3020 (10 and 20 MBq, respectively) was administered as a bolus injection and data were acquired by the microPET in 3×5 min time frames for each bed position starting 60 mins postinjection. To allow for all organs of interest (lung, liver, and kidney) to be scanned, 3–4 bed positions were used. The obtained imaging data were reconstructed into color-coded images describing the biodistribution of radioactivity in the rabbit. Regions of interest were delineated for lung, liver, and kidney to enable quantification of radiotracer concentration in these organs as described previously (9).

Table 2. *In Vitro* Quantification of ET_B Receptor Densities in Various Human Tissues Using [^{18}F]-BQ3020[a]

Lung	Kidney medulla	Kidney cortex	Heart
47.6 ± 6.2	33.1 ± 8.4	9.27 ± 0.7	5.5 ± 1.1

[a] As expected, high levels of ET_B receptors are expressed in lung and kidney medulla, whereas low levels are expressed in heart and kidney cortex. Values are mean ± SEM and are expressed as amol/mm^2. $n = 3$ per tissue.

Results

***In Vitro* Characterization.** Binding of [^{18}F]-BQ3020 to human left ventricle ($n = 4$) was concentration-dependent and saturable (Table 1). A one-site model was preferred to a two-site model and the Hill slope (nH) was close to unity. Binding of [^{18}F]-BQ3020 to human kidney ($n = 3$) was inhibited by ET-1 (1 μ*M*) and unlabeled BQ3020 (1 μ*M*), but not by the ET_A selective antagonist FR139317 (1 μ*M*). Quantitative autoradiography using [^{18}F]-BQ3020 revealed high levels of binding to ET_B receptors in lung and kidney medulla, whereas kidney cortex and heart showed lower levels of ET_B receptor densities (Table 2). In atherosclerotic coronary arteries, high levels of ET_B receptor densities were found to colocalize with macrophages (Fig. 1).

MicroPET Imaging. Following [^{18}F]-BQ3020 infusion, there was a rapid redistribution of radioligand from the circulation to ET_B receptor–rich tissue. High levels of [^{18}F]-BQ3020 binding were found in lung, liver, and kidney (Figs. 2 and 3). In kidney, a heterogeneous distribution of radioactivity was observed, with lower levels of uptake in the kidney cortex compared with the medulla (Figs. 2B and C, and 3), demonstrating that the microPET scanner has sufficient resolution to differentiate uptake in subrenal structures. As expected, ET_A-rich tissue in the heart could not be visualized in the microPET images.

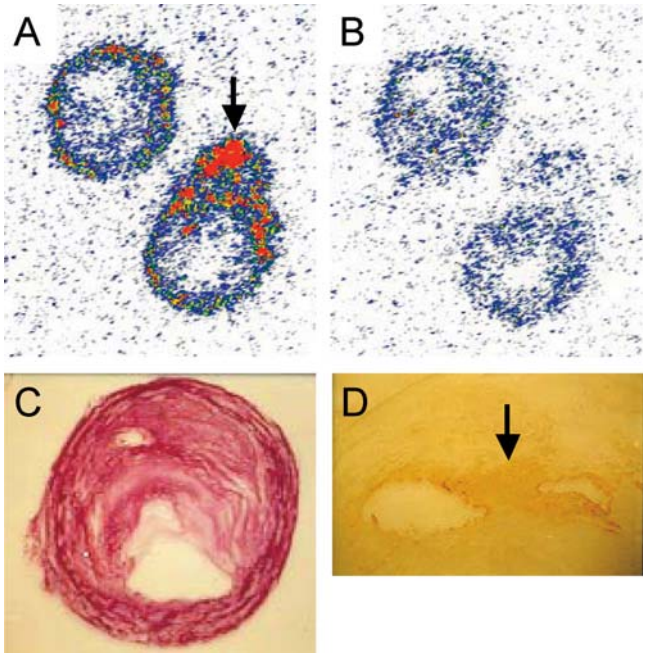

Figure 1. *In vitro* autoradiography showing (A) total and (B) nonspecific binding of [^{18}F]-BQ3020 in transverse sections of atherosclerotic coronary arteries. Images are color-coded to express level of radioactivity, with red indicating high levels and blue indicating low levels. (C) Hematoxylin and eosin–stained adjacent section showing the atherosclerotic plaque. (D) High densities of ET_B receptors were found to colocalize to areas with high densities of macrophages (arrows), as seen by macrophage staining using CD68 and the peroxidase-antiperoxidase technique yielding a brown reaction product.

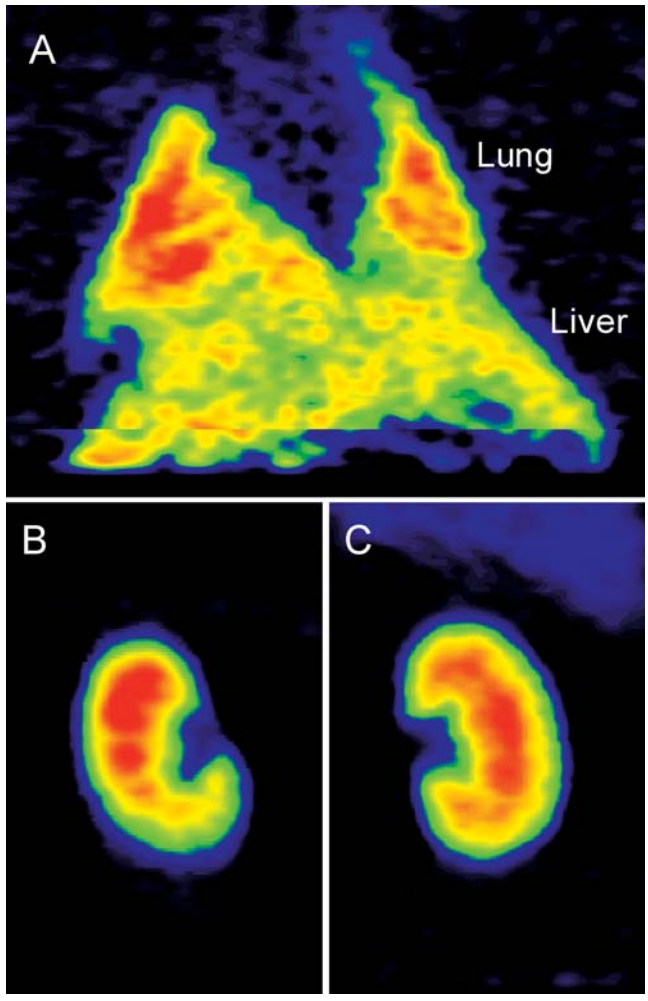

Figure 2. MicroPET images showing *in vivo* biodistribution of [^{18}F]-BQ3020 after intravenous infusion in New Zealand White rabbit (coronal planes). Images are color-coded to express level of radioactivity, with red indicating high levels and black/blue indicating low levels. (A) High levels of uptake were found in lung and liver. (B and C) In kidney, suborgan distribution of radioligand could be visualized with high levels of uptake in medulla and lower levels of uptake in cortex.

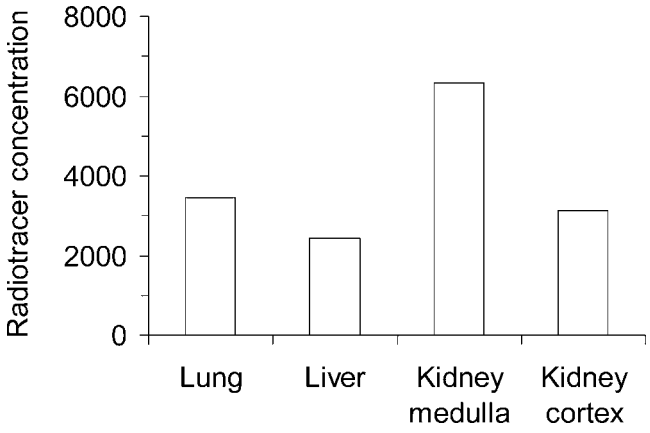

Figure 3. *In vivo* concentrations of [^{18}F]-BQ3020 in lung, liver, and substructures of kidney. Regions of interest were delineated in the microPET images to enable quantification of radiotracer concentration as described previously (9).

Discussion

We have demonstrated *in vitro* that [^{18}F]-BQ3020 has retained the expected subnanomolar affinity and selectivity to the ET_B receptor. Furthermore, we have shown using microPET that following infusion of [^{18}F]-BQ3020 the expected biodistribution of radioligand was obtained, with high levels of uptake in ET_B receptor–rich tissues in the rabbit.

We have previously shown that ^{18}F labeling of ET-1 in Lys^9 did not affect affinity and specificity for ET receptors (Table 1) and that [^{18}F]-ET-1 had the required pharmacokinetic properties to permit binding and imaging of ET receptors *in vivo* using microPET (1). We therefore hypothesized that using this approach for ^{18}F labeling of BQ3020 would not affect the affinity and selectivity to the ET_B receptor. *In vitro* characterization confirmed that [^{18}F]-BQ3020 had retained high-affinity binding with the expected single subnanomolar affinity comparable to values observed *in vitro* for [^{125}I]-BQ3020 (Table 1; Ref. 10). Binding was inhibited with ET-1 (mixed ET_A/ET_B) and BQ3020 (ET_B-selective) but not with FR139317 (ET_A-selective), demonstrating that [^{18}F]-BQ3020 had retained its selectivity for the ET_B receptor. High levels of binding were detected in lung and kidney medulla, tissue expressing high densities of ET_B receptors, whereas, as expected, heart and kidney cortex showed low levels of ET_B receptor densities (11). In atherosclerotic coronary arteries, [^{18}F]-BQ3020 binding was colocalized to macrophages, in agreement with the observation by Bacon *et al.* using [^{125}I]-BQ3020 (12), suggesting that [^{18}F]-BQ3020 potentially can be used for the visualization of atherosclerotic plaques *in vivo* with PET.

We have previously demonstrated, using dynamic microPET imaging, that [^{18}F]-ET-1 is rapidly cleared from the circulation by binding to ET receptors in lung, liver and kidney. This uptake was significantly blocked when the animal was pretreated with the ET_B selective antagonist BQ788, confirming that this fast clearance from the circulation was ET_B receptor–mediated (1). In support of these findings, we obtained a comparable biodistribution with high levels of uptake in lung, liver, and kidney when [^{18}F]-BQ3020 was infused in the rabbit, clearly demonstrating that the ET_B receptor plays an important role in the uptake of ET-1. In images reconstructed from the microPET, it was possible to delineate the expected heterogeneous distribution of ET_B receptor densities in the kidney, with high levels of [^{18}F]-BQ3020 binding in the medulla and low levels of binding in the cortex as demonstrated *in vitro* in this and previous studies (13), as well as *in vivo* using microPET and [^{18}F]-ET-1 (1).

In conclusion, this study shows that [^{18}F]-BQ3020 has retained high affinity and selectivity for the ET_B receptor and has the potential to image ET_B receptor distributions *in vivo* in normal and diseased tissue using positron emission tomography. In addition, the *in vivo* biodistribution of [^{18}F]-BQ3020 was comparable to that of [^{18}F]-ET-1, supporting our hypothesis that the ET_B receptor plays a significant role in the uptake of ET-1.

We thank Mrs. Rhoda Kuc for technical support.

1. Johnström P, Fryer TD, Richards HK, Harris NG, Barret O, Clark JC, Pickard JD, Davenport AP. Positron emission tomography using ^{18}F-labelled endothelin-1 reveals prevention of binding to cardiac receptors owing to tissue-specific clearance by ET_B receptors *in vivo*. Br J Pharmacol 144:115–122, 2005.
2. Johnström P, Harris NG, Fryer TD, Barret O, Clark JC, Pickard JD, Davenport AP. ^{18}F-Endothelin-1, a positron emission tomography (PET) radioligand for the endothelin receptor system: radiosynthesis and *in vivo* imaging using microPET. Clin Sci (Lond) 103(Suppl 48): 4S–8S, 2002.
3. Johnström P, Fryer TD, Richards HK, Barret O, Clark JC, Ohlstein EH, Pickard JD, Davenport AP. In vivo imaging of cardiovascular endothelin receptors using the novel radiolabelled antagonist [^{18}F]-SB209670 and positron emission tomography (microPET). J Cardiovasc Pharmacol 44(Suppl 1):S34–S38, 2004.
4. Johnström P, Aigbirhio FI, Clark JC, Downey SP, Pickard JD, Davenport AP. Syntheses of the first endothelin-A- and -B-selective radioligands for positron emission tomography. J Cardiovasc Pharmacol 36(Suppl 1):S58–S60, 2000.
5. Johnström P, Richards H, Fryer T, Barret O, Clark J, Pickard J, Davenport A. Radiosynthesis and *in vivo* biodistribution of [^{18}F]-Big ET-1, a potential PET radioligand for the study of enzyme conversion of Big ET-1 to ET-1. Br J Pharmacol 137:63P, 2002.
6. Johnström P, Davenport AP. Imaging and characterization of radioligands for positron emission tomography using quantitative phosphor imaging autoradiography. Methods Mol Biol 306:203–216, 2005.
7. Davenport AP, Kuc RE. Immunocytochemical localization of receptors using light and confocal microscopy with application to the phenotypic characterization of knock-out mice. Methods Mol Biol 306:155–172, 2005.
8. Davenport AP, Kuc RE. Radioligand-binding and molecular-imaging techniques for the quantitative analysis of established and emerging orphan receptor systems. Methods Mol Biol 306:93–120, 2005.
9. Johnström P, Fryer TD, Richards HK, Barret O, Davenport AP.

Dynamic in vivo imaging of receptors in small animals using positron emission tomography. Methods Mol Biol 306:217–232, 2005.

10. Molenaar P, Kuc RE, Davenport AP. Characterization of two new ET_B selective radioligands, [^{125}I]-BQ3020 and [^{125}I]-[Ala^{1,3,11,15}]ET-1 in human heart. Br J Pharmacol 107:637–639, 1992.
11. Davenport AP, Distribution of endothelin receptors. In: Huggins JP, Pelton JT, Eds. Endothelins in Biology and Medicine. Boca Raton: CRC Press Inc, p45, 1997.
12. Bacon CR, Cary NR, Davenport AP. Endothelin peptide and receptors in human atherosclerotic coronary artery and aorta. Circ Res 79:794–801, 1996.
13. Davenport AP, Morton AJ, Brown MJ. Localization of endothelin-1 (ET-1), ET-2, and ET-3, mouse VIC, and sarafotoxin S6b binding sites in mammalian heart and kidney. J Cardiovasc Pharmacol 17(Suppl 7): S152–S155, 1991.